第 11 卷 第 4 期 爆 炸 与 冲 击 Vol. 11, No. 4
1991 年 10 月 EXPLOSION AND SHOCK WAVES Oct., 1991

平面磁通量压缩流体动力学的数值模拟

L. L. Altgilbers, S. T. Wu, Y. C. Xiao
(美国阿拉巴马大学空间等离子体和高层大气物理研究中心和机械工程系,35899)

摘要 磁压缩发电机(MCGS)是一种应用炸药爆炸压缩导体包围的磁场,从而产生几百兆高斯强磁场并可作为初级能源,产生几百兆焦耳的能量和兆安培的电流。Chernyshev 等[1]指出如作为初级能源做某些应用,产生兆安培电流脉冲的上升时间的数量级必须要达到微秒量级,但典型的一端燃烧型(end-burn)的磁压缩发电机电流脉冲的上升时间要几百微秒,所以不能满足要求。1978 年 Pavlovskii 等[2]提出应用轴上(axial initiation)起爆的磁压缩发电机,其上升时间可大为缩短。本文为应用数值模拟方法研究一端燃烧型和轴上起爆型两种磁压缩发电机的物理过程。

计算模型根据磁流体动力学理论,用二维平面模型,并假设初始磁场均匀分布在等离子体内。假设($x=L$)的边界是固定的,在另一边界($x=0$)上加压力脉冲。对一端燃烧磁压缩发电机,压力脉冲作用在另一边界的底部,该边界以 v_* 向上运动。对轴上起爆的磁压缩发电机则压力均匀地加在另一边上。应用理想磁流体动力学方程式组

$$\frac{D\rho}{Dt}+\rho\nabla\cdot\vec{v}=0 \tag{1}$$

$$\rho\frac{D\vec{v}}{Dt}=-\nabla p+\frac{1}{4\pi}(\nabla\times\vec{B})\times\vec{B} \tag{2}$$

$$\frac{D}{Dt}\left(\frac{p}{\rho^{\gamma}}\right)=0 \tag{3}$$

$$\frac{\partial\vec{B}}{\partial t}=\nabla\times(\vec{v}\times\vec{B}) \tag{4}$$

$$\nabla\cdot\vec{B}=0 \tag{5}$$

和物态方程

$$T=\frac{\bar{\mu}p}{R\rho} \tag{6}$$

式中

$$\frac{D}{Dt}=\frac{\partial}{\partial t}+\vec{v}\cdot\nabla$$

$\rho, p, T, \vec{v}, \vec{B}, \bar{\mu}, R$ 和 γ 相应地为密度,压力,温度,速度,磁感应强度,平均原子量,理想气体常数和比热比。计算时忽略了耗散效应如扩散和热传导等,以及其它外力如重力等。

计算程序基本上根据新发展的 SINIL 格式,用拉氏网格,应用控制体积方法。气体动力性质用隐式格式,磁场用显式格式,可以用直角坐标或柱坐标。计算误差小于 0.5%,在 VAX8530 机上进行计算。文中列有程序框图和一些不同初始条件的计算结果的表格和图示。最后文中给出了关于结果的一些结论。

关键词 磁通量压缩 数值模拟

1990 年 10 月 5 日收到原稿。

A NUMERICAL MAGNETOHYDRODYNAMIC SIMULATION OF MAGNETIC FLUX COMPRESSION-PLANAR GEOMETRY

L. L. Altgilbers, S. T. Wu, Y. C. Xiao

(Center for Space Plasma and Aeronomic Research and Department of Mechanical Engineering The University of Alabama in Huntsville, Huntsville, Alabama 35899, U. S. A.)

ABSTRACT In this paper, a numerical model to simulate the magnetocumulative generators is proposed. This model is based on the fundamental theory of magnetohydrodynamics. A newly developed multidimensional time—dependent MHD code was presented and some preliminary numerical results were given.

KEY WORDS magnetic flux compression, numerical simulation

I. INTRODUCTION

Magnetocumulative Generators (MCGs) are explosive devices that have been used to generate extremely high magnetic fields (hundreds of megagauss) and as prime power sources that generate hundreds of megajoules of energy and megaamps of current. As pointed out by Chernyshev et al. [1], when the MCG is used as a prime power supply for certain applications, it may be necessary to generate megaamp current pulses with risetimes on the order of a microsecond. However, the typical end-burn type of MCG generates current pulses with risetimes of hundreds of microseconds. Various schemes have been developed for shortening the risetime of these generators to include the introduction of explosive opening switches and pulse forming networks. In 1978, Pavlovskii et al. [2] proposed an axial initiation scheme for detonating the MCG, which would shorten the risetime of the generator, thus reducing the requirements on the external circuitry.

In this study we used a numerical model to examine the physics associated with both the end—burn and axial type generators. This model is based on the fundamental theory of magnetohydrodynamics (MHD). The numerical technique used for this study is the newly developed Semi-Implicit-Non-Iterative-Lagrangian (SINIL) scheme.

I. THEORY

In order to simulate the end-burn and axial initiated MCGs, we have employed a two-dimensional planar geometry for this study and we assumed that an initial magnetic field is embedded in a uniform plasma. We assumed that one boundary ($x=L$) was held stationary and that a pressure pulse was applied on the opposite boundary ($x=0$). To simulate the end-burn generator, a pressure pulse was applied at the base of the left boundary, as shown in Figure 1a, and allowed to move up the boundary with a velocity v_z. For the axial type generator, the pressure pulse was applied uniformily along the length of the left boundary as shown in Figure 1b.

There is no plasma nor magnetic field outside the domain. While this physical description

does not accurately describe the actual operating conditions inside an MCG, it should provide us a simple case with which to test the code that has been developed.

The governing equations are the ideal MHD equations, which (in Gaussian units) can be expressed as follows:

Continuity

$$\frac{D\rho}{Dt} + \rho\nabla \cdot \vec{v} = 0 \tag{1}$$

Momentum

$$\rho \frac{D\vec{v}}{Dt} = -\nabla p + \frac{1}{4\pi}(\nabla \times \vec{B}) \times \vec{B} \tag{2}$$

Energy

$$\frac{D}{Dt}\left(\frac{p}{\rho^{\gamma}}\right) = 0 \tag{3}$$

Induction

$$\frac{\partial \vec{B}}{\partial t} = \nabla \times (\vec{v} \times \vec{B}) \tag{4}$$

$$\nabla \cdot \vec{B} = 0 \tag{5}$$

Equation of State

$$T = \frac{\bar{\mu} p}{R\rho} \tag{6}$$

where

$$\frac{D}{Dt} = \frac{\partial}{\partial t} + \vec{v} \cdot \nabla$$

$\rho, p, T, \vec{v}, \vec{B}, \bar{\mu}, R$, and γ are density, pressure, temperature, velocity, magnetic induction, mean atomic mass, ideal gas constant, and ratio of specific heats respectively. We have neglected dissipative effects such as diffusion and thermal conduction, as well as external forces other than those of electromagnetic origin (i.e., gravity).

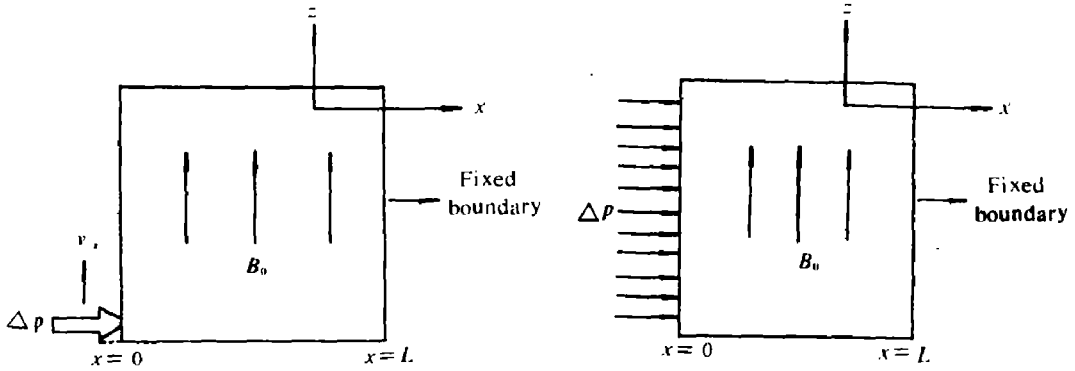

a. End burn type of MCG　　b. Axial-initiated MCG

Figure 1. pressure pulse applied to surface of plasma permeated with B_0.

Ⅱ. METHOD OF APPROACH

The MHD equations are coupled nonlinear partial differential equations, which are very complicated to solve. Therefore, a newly developed numerical scheme[3] is employed for this investigation. The numerical model is a time-dependent, nonlinear two-dimensional MHD model that incorporated gravitational and radiative losses. The corresponding numerical code is based on the newly developed SINIL scheme. The MHD equations are decretized on a Lagrangian grid, using the control-volume method. The gas dynamic properties are solved explicitly, and the magnetic field is solved implicitly without using numerical iterations. The numerical code can self-consistently simulate the interaction between the plasma fluids on both sides of an interface, in either cartesian or cylindrical coordinates and for any value of β (from as small as 10^{-4} to as large as ∞), where β is the ratio of the gas pressure to the magnetic pressure. Comparison with analytic results reveals that numerical errors are less than 0.5%.

To facilitate the implementation of the numerical scheme, the MHD equations have been rewritten in the following format:

$$\frac{D\rho}{Dt} = -\rho\nabla\cdot\vec{v} \tag{7}$$

$$\frac{D\vec{v}}{Dt} = -\frac{1}{\rho}\nabla\cdot\left[\left(\rho+\frac{B^2}{8\pi}\right)I\right]+\frac{1}{\rho}\nabla\cdot\left[\frac{\vec{B}\vec{B}}{4\pi}\right] \tag{8}$$

$$\frac{D}{Dt}\left[\frac{p}{\rho^\gamma}\right] = 0 \tag{9}$$

$$\frac{D\vec{B}}{Dt} = (\vec{B}\cdot\nabla)\vec{v} - \vec{B}(\nabla\cdot\vec{v}) \tag{10}$$

$$\nabla\cdot\vec{B} = 0 \tag{11}$$

$$T = \frac{\bar{\mu}p}{R\rho} \tag{12}$$

Where I is the unit tensor.

The numerical model was designed so as to give it the ability:

(a) to trace interfaces.

(b) to resolve self-consistently the interactions between internal (magnetized) and external (field-free) media.

(c) to study small β problems.

(d) to conserve energy.

(e) to handle small perturbations.

The numerical code was designed for a two-dimensional (x, z) planar problem, in which $\partial/\partial y = 0$ and the y—components of all the variables were assumed to be zero (e.g., $v_y = B_y = 0$). A Lagrangian computation grid was used. That is, the plasma is covered by a mesh of computational cells whose vertices move with the fluid. In this way, the fluid element in the interior of a cell always remains in that cell and the fluid boundaries always move with the cell bound-

aries. A sample computational mesh is shown in Figure 2a and the variables in an individual computational cell are shown in Figure 2b. A position vector and a velocity vector are assigned to each vertex, and values of the magnetic field, gas pressure, density, and temperature are assigned to each cell.

The boundaries in a numerical computation may be classified into two catagories[4]; i.e., physical boundaries and computational boundaries. The physical boundaries arise solely for physical reasons, while computational boundaries are boundaries imposed to limit the size of the computational domain. The boundaries for this problem are identified in Figure 3. The boundaries are 300 × 300 cm.

The computational flow diagram is presented in Figure 4. The computations were performed on a VAX8530.

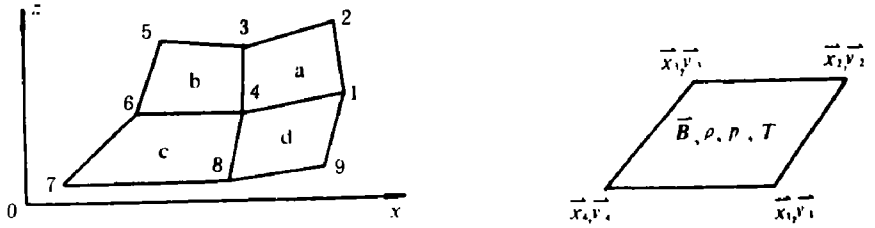

a. Sample grid points and computational cells　　b. Variables in cell "a"

Figure 2　Computational mesh

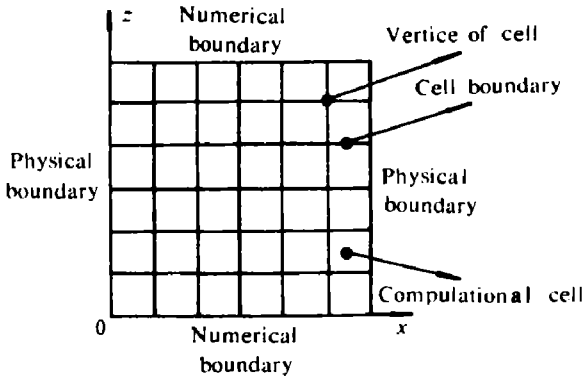

Figure 3　Boundaries of computational cell

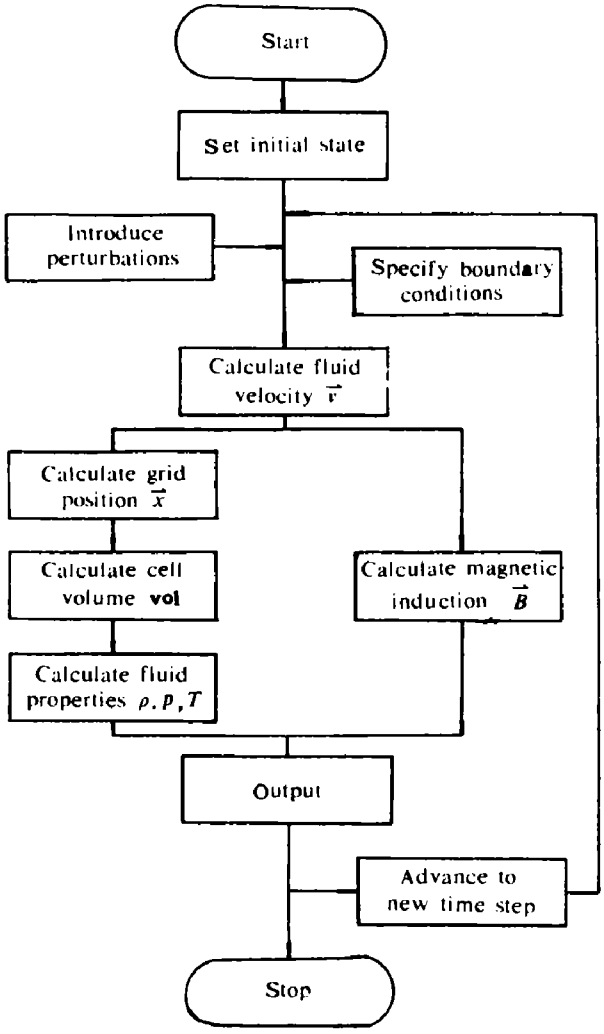

Figure 4 Computational flow diagram[3]

Ⅳ. NUMERICAL RESULTS

To obtain the numerical solution for the set of time—dependent nonlinear partial differential equations (i. e. , Equation (7)～(12)), we have to establish the initial conditions. These conditions must satisfy the governing equations. These initial conditions are:

(a)the magnetic field is a potential field configuration (i. e. , current free $\nabla \times \vec{B}=0$). The initial numerical values for the magnetic field strengths are $B_r=B_\theta=0$ and $B_z=B_0=10^3$, 10^4, and 10^5 Gauss (corresponding to Betas of 25. 13, 0. 2513 and 2. 513 $\times$ 10^{-3}, respectively)

(b) there is no plasma motion initially.

(c) the initial pressure is $p_0=10^5$Pa.

(d) the initial density is $\rho_0=$ 1. 3$\times10^{-3}$g/cm^3.

(e) the initial temperature is $T_0 = 300^0$K.

After these initial conditions have been established, a pressure pulse is exerted on the left boundary as shown in Figure 1. This pressure pulse generated a velocity in the x—direction of 100 cm/s. For the case of the end—burn type of MCG, the disturbance propagates up the left boundary with speeds of 10^6cm/s and 10^7 cm/s. For the case of the axial type MCG ($v_z = \infty$), the disturbance propagates uniformily outward along the length of the wall. The maximum and average current, magnetic energy, electric energy, magnetic field (B_z), magnetic field ratio ($(B_z - B_{z0})/B_{z0}$), pressure ratio ($(p - p_0)/p_0$), density ratio ($(\rho - \rho_0)/\rho_0$), temperature ratio ($(T - T_0)/T_0$), and velocity components in the x— and z— direction are calculated for various values of B_0, v_z, and times after initiation ($t = 360$, 3400, and 8000 μs). These results are summarized in Tables 1 and 2.

Based upon the data presented in Tables 1 and 2, the following general conculsions are proposed:

(a) As the velocity of the disturbances (v_z) decreases at some time t:

(i)the total current generated tends to decrease slightly for both types of generators.

(ii)the peak current density increases for the axial generator, but remains fairly constant for the end-burn generator.

(iii)the total energy generated tends to decrease slowly for both types of generators, while the peak energy tends to increase for the axial generator but remains constant in the end-burn types of generator.

(iv)the average and peak axial magnetic fields (B_z) tend to decrease in the axial generator, but remain fairly constant in the end-burn type of generator.

(b) As the initial magnetic field (B_0) decreases at some time t.

(i) the total current decreases for both types of generators, while the peak current density increases for the axial generator, but remains fairly constant for the end-burn type of generators.

(ii) the total energy generated tends to decrease, while the peak energy increases for the axial generator, but remains fairly constant for the end burn-type generators.

(iii) the average total axial magnetic field tends to decrease, while the peak axial magnetic field increases for the axial generator but remains fairly constant for the end-type generator.

(c) The ratio of the thermal energy to magnetic energy increases as B_0 decreases and as β increases.

Figures 5 and 6 and plots of the magnetic energy and current density in the x,z plane 360 μs after applying the pressure pulse for various values of the initial magnetic field and the velocity of the disturbance (v_z) along the left wall of the control volume. From these diagrams the following observations can be made:

(a) As the initial magnetic field decreases the rise time of the generated pulse increases, but the speed at which the pulse propagates into the plasma decreases . This latter observation is

Table 1 Values of various parameters calculated for different values of B_0 and v_s

			Currents		E—Magnetic		E—Thermal		E—Kinetic		E—Total	
* B_0	* v_s	* t	Total	max density	total	max density	total	max density	total	max density	total	max density
Gauss	cm/s	μs	A	A/cm²	J	10^{-7}J/cm³	J	10^{-7}J/cm³	J	10^{-7}J/cm³	J	10^{-7}J/cm³
10^5	∞	360	7.0×10^4	1.0×10^2	5.4×10^{-2}	10	1.1×10^{-4}	0.02	5.4×10^{-2}	10	1.1×10^{-1}	20
10^5	10^7	360	7.0×10^4	1.2×10^2	5.2×10^{-2}	15	1.1×10^{-4}	0.03	5.2×10^{-2}	14	1.0×10^{-1}	29
10^5	10^6	360	3.2×10^5	1.9×10^2	3.6×10^{-2}	43	$8.\times10^{-5}$	0.08	2.6×10^{-2}	38	6.3×10^{-2}	55
10^4	∞	3400	8.3×10^4	1.0×10^2	4.7×10^{-2}	8.7	8×10^{-3}	1.8	5.6×10^{-2}	10	1.1×10^{-1}	21
10^4	10^6	3400	7.0×10^4	1.2×10^2	4.5×10^{-2}	12	9.4×10^{-2}	2.5	5.4×10^{-2}	15	1.1×10^{-1}	29
10^4	∞	360	9.7×10^2	9.7×10	4.4×10^{-3}	7.4	9.3×10^{-4}	1.6	5.1×10^{-3}	8.4	1.0×10^{-2}	1.7
10^4	10^7	360	9.0×10^2	9.7×10	4.7×10^{-3}	8.6	9.1×10^{-4}	1.8	5.0×10^{-3}	9.1	1.0×10^{-2}	19
10^4	10^6	360	3.87×10^3	8.6×10	2.5×10^{-3}	8.26	5.2×10^{-4}	1.75	2.7×10^{-3}	8.6	5.7×10^{-3}	18.5
10^3	∞	8000	8.0×10^4	1.0×10^2	2.6×10^{-3}	0.47	5.4×10^{-2}	10	5.6×10^{-2}	10	1.1×10^{-1}	20
10^3	∞	3400	3.0×10^4	1.0×10^2	1.1×10^{-3}	0.47	2.3×10^{-2}	10	2.4×10^{-2}	9.6	4.8×10^{-2}	20
10^3	10^6	3400	2.8×10^4	1.0×10^2	1.05×10^{-3}	0.47	2.2×10^{-2}	10	2.3×10^{-2}	9.9	4.6×10^{-2}	20
10^3	∞	360	3.2×10^3	8.6×10	8.4×10^{-5}	0.4	1.8×10^{-3}	8.6	1.7×10^{-3}	7.5	3.5×10^{-3}	17

* B_0=Initial magentic field;

v_s=Speed of pressure pulse along the wall at $x=0$;

t=Time after initiation of high explosive.

Table 2　Values of various parameters calculated for different values of B_0 and v_s

			$(B_z-B_z^0)/B_0^0$		B_z		$(p-p^0/p^0)$		$(\rho-\rho^0/\rho^0)$		$T-T^0/T^0)$		V_r		V_z	
* B_0	* v_s	* t	ave	max	ave	max	ave	max	ave	max	ave	max	ave	max	ave	max
Gauss	cm/s	μs	10^{-4}	10^{-4}	Gauss	Gauss	10^{-4}	10^{-4}	10^{-4}	10^{-4}	10^{-4}	10^{-4}	cm/s	cm/s	cm/s	cm/s
10^5	∞	360	1.2	1.6	0	1	2.0	2.7	1.2	1.6	0.8	1.1	0	0	93	126
10^5	10^7	360	1.14	1.9	0.37		2.0	3.2	1.1	1.9	0.8	1.3	0.014	0.37	90	151
10^5	10^6	360	0.7	3.3	3.4		1.15	5.2	0.7	3.1	0.5	2.1	0.09	2.5	55	244
10^4	∞	3400	11	15	0		19	2.5	11	15	7.5	9.8	0	0	97	127
10^4	10^8	3400	11	17	0.4		18	29	11	17	7.2	12	1.3	6.4	93	153
10^4	∞	360	11	14	0		1.8	22	1.1	14	0.72	19.1	0	0	9.5	122
10^4	10^7	360	11	15	0.006		1.8	25	1.1	15	0.71	10	0.01	3.9	9.3	125
10^4	10^6	360	0.62	14	0.05		1	24	0.62	14.5	0.4	10	0.08	5.8	5.6	123
10^3	∞	8000	26	35	0		44	58	26	35	18	23	0	0	97	127
10^3	∞	3400	11	34	0		19	58	11	34.5	7.4	23	0	0	41	126
10^3	10^6	3400	11	34	0.04		18	58	11	35	7.2	23	1.3	10	40	127
10^3	∞	360	0.92	32	0		1.5	54	0.9	32	0.6	21	0	0	3.6	111

* B_0 = Initial magnetic field; v_s = Speed of pressure pulse along the wall at $z=0$; t = Time after initiation of high explosive.

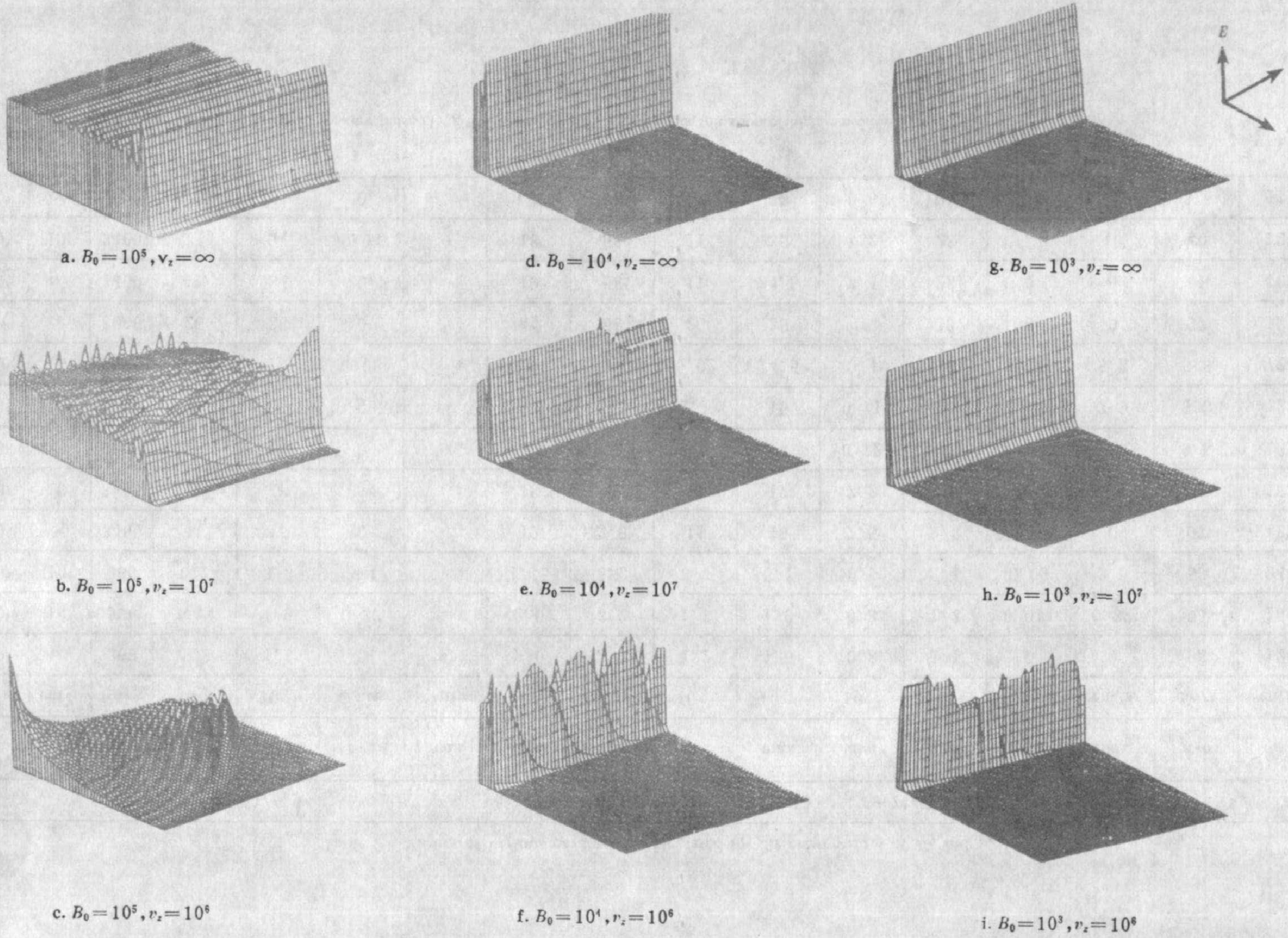

a. $B_0=10^5, v_z=\infty$　　d. $B_0=10^4, v_z=\infty$　　g. $B_0=10^3, v_z=\infty$

b. $B_0=10^5, v_z=10^7$　　e. $B_0=10^4, v_z=10^7$　　h. $B_0=10^3, v_z=10^7$

c. $B_0=10^5, v_z=10^6$　　f. $B_0=10^4, v_z=10^6$　　i. $B_0=10^3, v_z=10^6$

Figure 5　Magnetic energy calculated of $t=360$ μs for various initial magnetic fields and perturbation velocities

Figure 6. current densities calculated at $t=360$ μs for various initial magnetic fields and perturbation velocities

expected since the magnetosonic (or fast) velocity is directly proportional to the initial magnetic field stength.

(b) The current and magnetic energy generated are very sensitive to the value of the ratio of v_z/v_{fast} (where v_{fast} is the magnetosonic velocity) especially when $v_z/v_{fast}<1$.

(c) The axial generator provides for uniform compression of the initial magnetic field.

V. CONCLUSION

In this study, a newly developed multi-dimensional time-dependent MHD code using the SINIL scheme was presented with some preliminary numerical results for the modelling of plasma motions in a planar geometry for end-burn and axial-burn type MCG' s. From these preliminary results, it is shown that the numerical scheme employed is reasonably stable and that it has the ability to handle extremely low β—plasma problems.

The calculations show that axial initiation does result in a faster risetime as suggested by Pavlovskii et al. [2]. It is also apparent that the axially—initiated generator provides for a uniform compression of the magnetic field and generation of energy, which may result in simplifying MCG designs. Future studies will involve looking at cylindrical designs and incorporating such nonlinear effects as magnetic field diffusion into the walls of the MCG.

REFERENCES

[1] Chernyshev, V. K., Volkov, G. S., Ivanov, V. A., Vakhrushev, V. V., "Study of Basic Regularities of Formation of Multi—MA—Current Pulses with Short Risetime by EMG Circuit Interruption", Megagauss Physics and Technology, Edited by Peter J. Turchi, Plenum Press, New York, (1980), 163—675.

[2] Pavlovskii, A. I., Lyudaev, R. Z., Zolotov, V. A., Seryaghin, A. S., Yuryzhev, A. S., Kharlamov, M. M., Shuvalov, A. M., Gurin, V. Ye., Spirov, G. M., and Makaev, B. S., "Magnetic Cumulation Generator Parameters and Means to Improve Them", Megagauss Physics and Technology, Edited by Peter J. Turchi, Plenum Press, New York, (1988), 557—583.

[3] Ying Cai Xiao, "A Numerical Model for the Study of Magnetohydrodynamic (MHD) Waves in a Structured Medium", Ph. D. Thesis, Department of Physics, The University of Alabama in Huntsville, (1988).

[4] Hu, Y. Q., Wu., S. T., *J. of Computational Physics*, **55** (1984), 33.